


ORIGINAL ARTICLE

Open Access



The value of restriction spectrum imaging in predicting lymph node metastases in rectal cancer: a comparative study with diffusion-weighted imaging and diffusion kurtosis imaging

Huijia Yin¹, Wenling Liu¹, Qin Xue¹, Chen Song², Jipeng Ren¹, Ziqiang Li¹, Dongdong Wang³, Kaiyu Wang⁴, Dongming Han^{1*} and Ruifang Yan^{1*} 

Abstract

Background To investigate the efficacy of three-compartment restriction spectrum imaging (RSI), diffusion kurtosis imaging (DKI), and diffusion-weighted imaging (DWI) in the assessment of lymph node metastases (LNM) in rectal cancer.

Methods A total of 77 patients with rectal cancer who underwent pelvic MRI were enrolled. RSI-derived parameters (f_1 , f_2 , and f_3), DKI-derived parameters (D_{app} and K_{app}), and the DWI-derived parameter (ADC) were calculated and compared using a Mann–Whitney U test or independent samples t -test. Logistic regression (LR) analysis was used to identify independent predictors of LNM status. Area under the receiver operating characteristic curve (AUC) and Delong analysis were performed to assess the diagnostic performance of each parameter.

Results The LNM-positive group exhibited significantly higher f_1 and K_{app} levels and significantly lower f_3 , D_{app} , and ADC levels compared to the LNM-negative group ($p < 0.05$). There was no difference in f_2 levels between the two groups ($p = 0.783$). LR analysis showed that D_{app} and K_{app} were independent predictors of a positive LNM status. AUC and Delong analysis showed that DKI ($D_{app} + K_{app}$) exhibited significantly higher diagnostic efficacy (AUC = 0.908; sensitivity = 87.10%; specificity = 86.96%) than RSI ($f_1 + f_3$) and DWI (ADC), with AUCs were 0.842 and 0.771 ($Z = 2.113$, 3.453; $p = 0.035$, < 0.001 , respectively). The AUC performance between RSI and DWI was also statistically significant ($Z = 1.972$, $p = 0.049$).

Conclusion The RSI model is superior to conventional DWI but inferior to DKI in differentiation between LNM-positive and LNM-negative rectal cancers. Further study is needed before it could serve as a promising biomarker for guiding effective treatment strategies.

Critical relevance statement The three-compartment restriction spectrum imaging was able to differentiate between LNM-positive and LNM-negative rectal cancers with high accuracy, which has the potential to serve as a promising biomarker that could guide treatment strategies.

*Correspondence:

Dongming Han
625492590@qq.com
Ruifang Yan
yrf718@163.com

Full list of author information is available at the end of the article



© The Author(s) 2024. **Open Access** This article is licensed under a Creative Commons Attribution 4.0 International License, which permits use, sharing, adaptation, distribution and reproduction in any medium or format, as long as you give appropriate credit to the original author(s) and the source, provide a link to the Creative Commons licence, and indicate if changes were made. The images or other third party material in this article are included in the article's Creative Commons licence, unless indicated otherwise in a credit line to the material. If material is not included in the article's Creative Commons licence and your intended use is not permitted by statutory regulation or exceeds the permitted use, you will need to obtain permission directly from the copyright holder. To view a copy of this licence, visit <http://creativecommons.org/licenses/by/4.0/>.

Key Points

- Three-compartment restriction spectrum imaging could differentiate lymph node metastases in rectal cancer.
- Diffusion kurtosis imaging and diffusion-weighted were associated with lymph node metastases in rectal cancer.
- The combination of different parameters has the potential to serve as a promising biomarker.

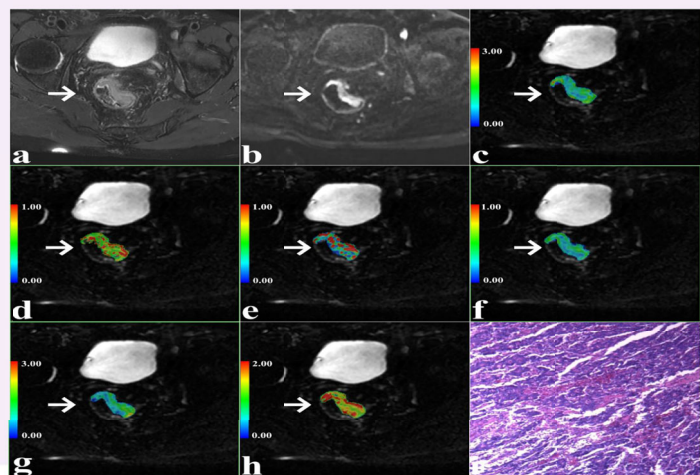
Keywords Rectal cancer, Lymph node metastases, Restrictive spectrum imaging, Diffusion kurtosis imaging, Diffusion-weighted imaging

Graphical Abstract

The value of restriction spectrum imaging in predicting lymph node metastases in rectal cancer: a comparative study with diffusion-weighted imaging and diffusion kurtosis imaging

ESIRI¹ EUROPEAN SOCIETY OF RADIOLOGY

The three-compartment restriction spectrum imaging (RSI) model was able to differentiate between LNM-positive and LNM-negative rectal cancers. Compared to conventional DWI, the RSI model exhibited superior diagnostic performance, but weaker than that of DKI. These findings suggest that the RSI model has the potential to serve as a promising biomarker for guiding effective treatment strategies.



Insights
into Imaging

Insights Imaging (2024) Yin H, Liu W, Xue Q et al.
DOI: /10.1186/s13244-024-01852-z

Introduction

Rectal cancer has emerged as the fourth most prevalent form of cancer worldwide and the second leading cause of mortality [1, 2]. Clinical interventions for rectal cancer, such as surgical excision and neoadjuvant chemoradiotherapy, can lead to significant adverse events in the absence of a precise assessment of lymph node metastasis (LNM) status [3, 4]. Smith et al demonstrated that LNM was correlated with a poorer prognosis, even in cases of complete regression of the primary tumor, and the rate of recurrence was notably higher in LNM-positive patients compared to LNM-negative [5]. Therefore, accurate pre-operative evaluation of LNM is essential for guiding treatment strategies and improving clinical outcomes in individuals with rectal cancer.

Currently, clinical practitioners rely on highly invasive biopsy procedures to determine the LNM status of rectal cancer, which carries risks and complications. Magnetic

resonance imaging (MRI) has been widely recommended as a non-invasive tool to evaluate LNM status [6]. However, morphological assessment has been associated with low sensitivity and specificity [7]. Diffusion-weighted imaging (DWI) is a well-known diffusion MRI technique, and several studies have shown that its quantitative parameter, the apparent diffusion coefficient (ADC), has a positive role in the differential diagnosis of LNM in rectal cancer [8, 9]. However, DWI relies on accurately measuring the diffusion motion of water molecules using Gaussian distribution, limiting the diagnostic accuracy [10, 11]. Diffusion kurtosis imaging (DKI), another diffusion MRI technique based on the theory of a non-Gaussian distribution of water molecules in tissues, was first proposed by Jensen et al in 2005 [12]. In contrast to traditional DWI, DKI comprehensively accounts for the complex nature of water molecule diffusion within tissues by incorporating fourth-order 3-dimensional tensors into the original diffusion imaging model. This improves the

precision in the quantitative evaluation of diffusion characteristics in tissues, thereby capturing the nuanced complexity of tissue microstructure with increased sensitivity [13, 14]. Currently, few studies have directly compared the differences in DKI-related parameters between metastatic and non-metastatic lymph nodes in rectal cancer from the perspective of the primary lesion, presenting challenges in the development of a comprehensive reference for clinical diagnosis and treatment [15, 16].

Restriction spectrum imaging (RSI) is a cutting-edge diffusion model employed in MRI that effectively categorizes water diffusion into distinct microscopic tissue compartments, such as restricted, hindered, and free water compartments, by fitting signals to a linear combination of diffusion-weighted models [17]. To date, RSI has demonstrated initial promise in the evaluation of various diseases, including prostate cancer [18] and breast cancer [19]. But to our knowledge, in the field of rectal cancer, only Xiong et al have assessed tumor grading using RSI [20].

Therefore, this study aims to explore the diagnostic value of three-compartment RSI in the assessment of

LNM in rectal cancer, and compare it with DKI and DWI, with a view to providing novel imaging markers for accurate clinical diagnosis and to guide treatment strategies to improve clinical outcomes.

Materials and methods

Study population

The current study was approved by the local ethics committee, and all participants provided written informed consent. Between March 2023 and May 2024, a total of 100 patients underwent pelvic MRI due to suspected rectal cancer following clinical evaluation. The exclusion criteria were as follows: (1) patients with pathologically confirmed non-rectal cancer ($n = 5$); (2) patients with inconclusive pathological results ($n = 4$); (3) patients with a time interval of more than 2 weeks between scanning and biopsy ($n = 3$); (4) patients who did not complete all MRI scans or whose images were of insufficient quality for analysis ($n = 6$); and (5) patients who had undergone relevant treatment prior to the scans ($n = 5$). Consequently, 77 patients were enrolled in the study (Fig. 1).

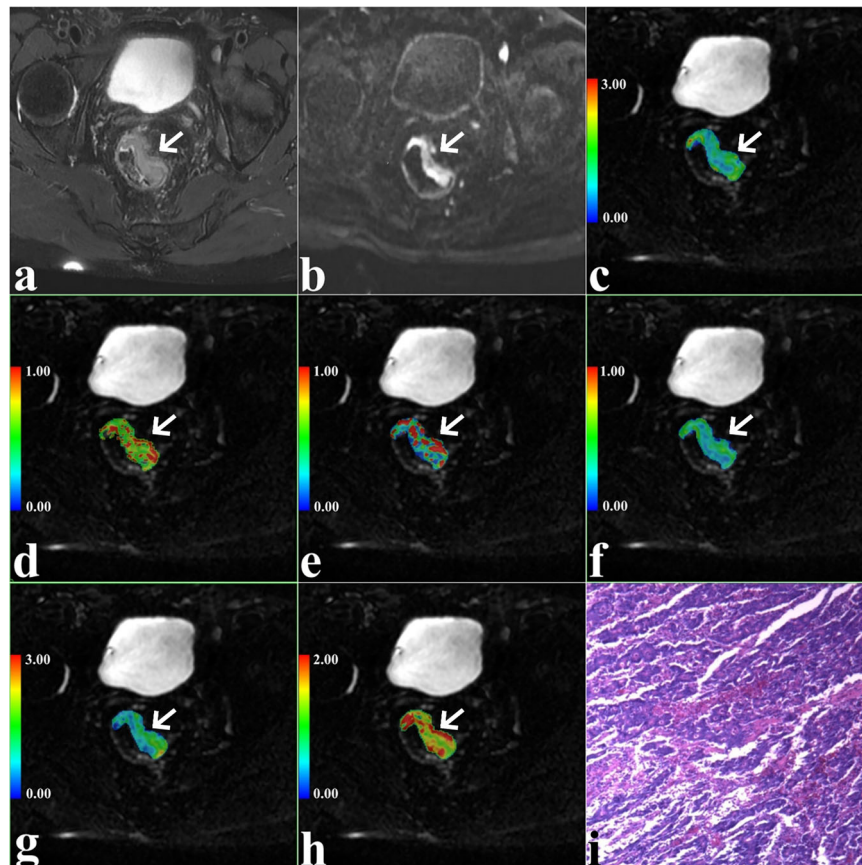


Fig. 1 A 67-year-old man with LNM-positive rectal cancer in the left wall of rectum (arrow, pseudo colored region). T2-weighted image showed a slightly hyperintensity mass (a) with restricted diffusion on DWI (b) ADC map (c). d–h f_1 , f_2 , f_3 , D_{app} , and K_{app} maps of the same slice as in a–c. i Pathological image (original magnification, $\times 100$)

Patient characteristics, including age, gender, maximum tumor diameter, and CEA levels, were recorded.

Image acquisition

A 3.0-Tesla MRI system (Signa Architect, GE Medical Systems, Milwaukee, WI) equipped with a 16-channel phased-array body coil was utilized for pelvic imaging. Prior to the scan, all patients had their rectums emptied and were given anti-peristalsis medication when appropriate. All patients were placed in the supine position, feet-first into the scanner. Initially, a T2-weighted imaging (T2WI) sequence in the axial plane was conducted to delineate the tumor location that employed the following parameters: repetition time/echo time (TR/TE) = 4600/125 ms; slice thickness = 3 mm; gap = 0.3 mm; number of excitations (NEX) = 2; field of view (FOV) = 360 × 360 mm; and matrix = 268 × 320. The T2WI resulted in a total scan time of 2 min 49 s. Subsequently, using T2WI as a reference, multiple b-value sequences were performed for the slices containing the lesions. The scanning position, layer thickness, and gap of the b-value sequences remained unchanged, and the following parameters were used: TR/TE = 445/85.3 ms; slice thickness = 3 mm; gap = 0.3 mm; b-values = 0, 50, 100, 150, 200, 400, 600, 800, 1000, 1500, and 2000 s/mm²; NEX = 1, 1, 1, 1, 1, 2, 2, 2, 4, 4, and 4; FOV = 360 × 360 mm; and matrix 128 × 128. This resulted in a total scan time of 4 min 55 s.

Parameter generation

All analyses were performed using Matlab R2018b (MathWorks Inc., Natick, MA, USA). Preceding the quantitative analysis, the raw data from the b-value sequences underwent various corrections to address B₀ distortion, gradient nonlinearities, and eddy current distortions. The DWI is expressed using the following equation:

$$S_b/S_0 = \exp(-b \times \text{ADC}) \quad (1)$$

where ADC is the apparent diffusion coefficient, b is the diffusion sensitizing factor, and S₀ and S_b are the signal intensities under different b-values (0 s/mm² and 800 mm²/s, respectively) [8].

The DKI is expressed using the following equation:

$$S_b = S_0 \times \exp\left(-b \times D_{\text{app}} + b^2 \times D_{\text{app}}^2 \times K_{\text{app}}/6\right) \quad (2)$$

where K_{app} is kurtosis, representing the deviation from the Gaussian distribution, while D_{app} is diffusivity, representing the diffusion coefficient corrected for non-Gaussian bias [12].

The RSI is expressed using the following equation:

$$S(b) = f_1 e^{-bD1} + f_2 e^{-bD2} + f_3 e^{-bD3}, D1 < D2 < D3 \quad (3)$$

where f₁, f₂, and f₃ are the volume fractions of restricted diffusion, hindered diffusion, and free water diffusion compartments, respectively, and D1, D2, and D3 are the ADCs of the corresponding compartments. To prevent overfitting, ensure the linearization of the RSI model, and maintain comparability of volume fractions across compartments, according to the theoretical values and experimental findings, D1, D2, and D3 were standardized to 0.5 × 10⁻³ mm²/s, 1.3 × 10⁻³ mm²/s, and 3.0 × 10⁻³ mm²/s, respectively [20].

All the parameters included in this study were derived from the primary tumor. Two independent radiologists who were blinded to histopathologic and clinic data determined the whole-tumor volume by manually analyzing regions of interest (ROIs) along the tumor's outer edge on DWI images using ITKSNAP software (version 3.8.0; <http://www.itksnap.org>). Obvious cystic, necrotic, hemorrhagic, and calcified regions were avoided by referencing the corresponding T2WI images. Subsequently, the whole-tumor ROIs were automatically transferred to the parametric maps (including ADC, D_{app}, K_{app}, f₁, f₂, and f₃), followed by the calculation of parametric values.

Histopathological evaluation

All specimens were obtained by surgical resection of the primary tumor and nodal dissection, and the median interval from MRI examination to surgery was 11 days (1–14 days). All resected samples were fixed in formalin, dehydrated, immersed in wax, embedded in paraffin, sectioned, and stained with hematoxylin and eosin (H&E). Pathologic staging was performed according to the guidelines outlined in the Eighth Edition American Joint Committee on Cancer Staging Manual [21]. Patients with one or more lymph node metastases were assigned to the LNM-positive group, otherwise the LNM-negative group.

Statistical analysis

Interclass correlation coefficients (ICC) were calculated to evaluate interobserver agreement for DKI, RSI, and DWI parameters, with ICCs > 0.75 indicating excellent reliability [22]. Differences between the LNM-positive and LNM-negative groups were analyzed using a Mann–Whitney *U* test, independent samples *t*-test, or chi-square test based on the distributional properties of the variables. The diagnostic performance of DKI, RSI, and DWI was evaluated using the area under the receiver operating characteristic curve (AUC). The deLong test was used to compare the differences in AUCs of each parameter. Logistic regression (LR) analysis was employed to identify independent influencing factors and combined diagnostic assessments. Statistical analyses were conducted using MedCalc software (version 15.0;

Table 1 Comparison of different variables among different groups

Variables	LNM-positive (n = 31)	LNM-negative (n = 46)	t / χ^2 / z value	p-value
Age (years)*	63.54 ± 10.03	60.68 ± 10.85	1.171	0.246 ^a
Maximum diameter (cm)*	4.24 ± 1.39	3.83 ± 1.26	-1.298	0.199 ^a
Sex, n (%)			2.542	0.111 ^c
Male	16 (51.61%)	32 (69.57%)		
Female	15 (48.39%)	14 (30.43%)		
CEA (ng/mL) [#]	4.08 (1.84, 13.35)	2.68 (1.21, 6.02)	-1.828	0.068 ^b
f ₁ [#]	0.43 (0.35, 0.50)	0.21 (0.09, 0.38)	-5.027	< 0.001 ^b
f ₂ [#]	0.12 (0.07, 0.19)	0.13 (0.06, 0.22)	-0.275	0.783 ^b
f ₃ [#]	0.27 (0.20, 0.30)	0.36 (0.28, 0.55)	-3.454	0.001 ^a
D _{app} (× 10 ⁻³ mm ² /s)*	1.04 ± 0.44	1.85 ± 0.07	5.802	< 0.001 ^a
K _{app} [*]	0.77 ± 0.27	0.49 ± 0.18	-5.322	< 0.001 ^a
DWI / ADC (× 10 ⁻³ mm ² /s)*	1.09 ± 0.29	1.57 ± 0.62	4.550	< 0.001 ^a

LNM lymph node metastasis

* Data are means ± SDs

[#] Data are medians, with IQRs in parentheses^a Independent t-test^b Chi-squared test^c Mann-Whitney U test

MedCalc Software, Ostend, Belgium). *p*-values less than 0.05 were considered statistically significant.

Results

Patient characteristics

A total of 77 patients, 31 patients with LNM-positive and 46 LNM-negative rectal cancer were included. No statistically significant differences between the two groups were observed in age, gender, maximum diameter, or CEA levels (*p* > 0.05, Table 1).

Consistency evaluation

The measurements of D_{app}, K_{app}, ADC, f₁, f₂, and f₃ by the two observers showed excellent consistency, with all ICC values exceeding 0.75. The average readings from both observers were utilized for subsequent analysis.

Parameter comparison

The LNM-positive group exhibited significantly higher f₁ and K_{app} values and significantly lower f₃, D_{app}, and ADC values compared to the LNM-negative group (*p* < 0.05). However, the disparity in f₂ values between the two groups did not reach statistical significance (*p* = 0.783; Table 1; Fig. 2).

LR analysis

Age, gender, maximum diameter, CEA levels, D_{app}, K_{app}, ADC, f₁, f₂, and f₃ were all included in the LR analysis.

Univariate analysis demonstrated that CEA levels, f₁, f₃, D_{app}, K_{app}, and ADC were all independent predictors of LNM status (aP < 0.05). Further multivariate analysis demonstrated that only D_{app} (*p* = 0.034) and K_{app} (*p* = 0.004) were significantly correlated with a positive LNM status in rectal cancer patients (Table 2).

Diagnostic performance

Among the included parameters, K_{app} demonstrated the highest diagnostic efficacy (AUC = 0.874; sensitivity = 83.87%; specificity = 82.61%). The AUCs for D_{app}, f₁, ADC, and f₃ were 0.860, 0.839, 0.771, and 0.733, respectively. There is a statistically significant difference in AUCs between K_{app} and ADC (*Z* = 2.047, *p* = 0.041), and between K_{app} and f₃ (*Z* = 2.131, *p* = 0.033). Among the different diffusion models, DKI (D_{app} + K_{app}) exhibited the highest diagnostic efficacy (AUC = 0.908; sensitivity = 87.10%; specificity = 86.96%), which was significantly higher than RSI (f₁ + f₃) and DWI (ADC) (AUC = 0.842, 0.771; *Z* = 2.113, 3.453; and *p* = 0.035, < 0.001, respectively). Furthermore, there was a significant difference in AUC between RSI and DWI (*Z* = 1.972, *p* = 0.049). The diagnostic performances are summarized in Fig. 3 and Table 3.

Discussion

In this study, we demonstrated that the RSI-derived parameters (f₁, f₃), DKI-derived parameters (D_{app}, K_{app}), and DWI-derived parameter (ADC) could be used to distinguish LNM-positive from LNM-negative rectal cancer. The multivariate analysis showed that D_{app} and K_{app} were independent factors correlated with a positive TMN status. In addition, the DKI (D_{app} + K_{app}) model exhibited optimal diagnostic efficacy, which was significantly higher than those of the RSI (f₁ + f₃) and DWI (ADC) models, and the diagnostic efficacy of RSI (f₁ + f₃) model was significantly higher than DWI model.

DWI is a classical MRI diffusion imaging technique that models the diffusion of water molecules in biological tissues as a uniform Gaussian distribution [23]. In this study, the ADC values of LNM-positive patients were significantly lower than those of LNM-negative patients. These results are in line with previous studies that found that reduced ADC values were correlated with restricted internal water molecules leading to higher malignancy and more tightly organized structures in LNM-positive lesions [8, 9]. Therefore, the results of the present study provide evidence of the value of DWI in diagnosing the LNM status of rectal cancer.

Three-compartment RSI classifies the diffusion of water molecules in biological tissues into diffusion (f₁), hindered diffusion (f₂), and free-water diffusion (f₃) [18]. The f₁ refers to the retention of water molecules within a restricted space, f₂ denotes the passage delay of smaller molecules

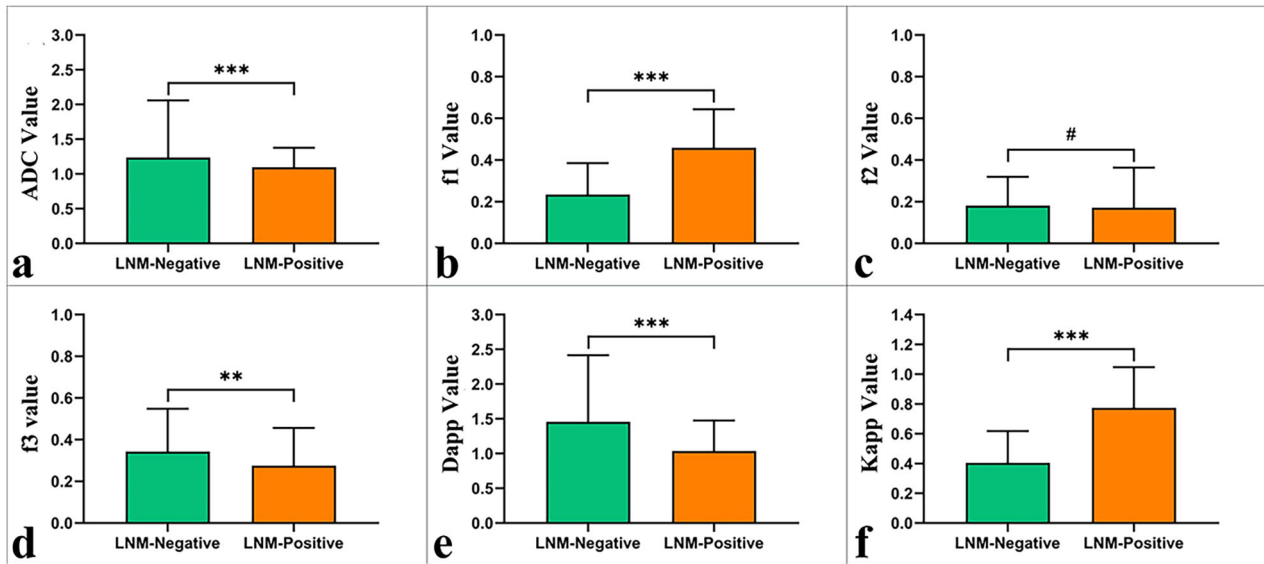


Fig. 2 Boxplots of various parameters in LNM-positive and LNM-negative rectal cancer: **a** ADC; **b** f_1 ; **c** f_2 ; **d** f_3 ; **e** D_{app} ; and **f** K_{app} . *** $p < 0.001$, ** $p < 0.01$, and # $p > 0.05$

Table 2 Univariate and multivariate analyses

Parameters	Univariate analyses		Multivariate analyses	
	OR* (95% CI)	p-value	OR* (95% CI)	p-value
Age (years)	0.755 (0.473–1.205)	0.239	/	/
Sex	0.467 (0.182–1.199)	0.113	/	/
Maximum diameter (mm)	1.365 (0.857–2.173)	0.190	/	/
CEA (ng/mL)	3.084 (0.868–10.959)	0.082	2.586 (0.283–23.657)	0.400
f_1	6.974 (2.703–17.994)	< 0.001	0.773 (0.126–4.754)	0.781
f_2	1.062 (0.675–1.673)	0.794	/	/
f_3	0.411 (0.220–0.767)	0.005	0.459 (0.174–1.207)	0.114
D_{app} ($\times 10^{-3}mm^2/s$)	0.104 (0.034–0.318)	< 0.001	0.065 (0.005–0.814)	0.034
K_{app}	17.780 (4.646–68.043)	< 0.001	12.989 (2.224–75.854)	0.004
ADC ($\times 10^{-3}mm^2/s$)	0.194 (0.074–0.513)	0.001	5.220 (0.987–27.607)	0.052

All factors with $p < 0.1$ in univariate analyses were included in multivariate regression analyses

OR odds ratio, CI confidence interval

* OR for per 1 standard deviation

when they traverse a cellular impediment, and f_3 delineates the random motion of water molecules in the absence of any obstacle [24]. The findings of the current study demonstrated the potential utility of RSI-derived parameters in differentiating between LNM-positive and LNM-negative rectal cancer. Specifically, LNM-positive rectal cancer exhibited a higher f_1 and a lower f_3 value compared to LNM-negative. This may be attributed to an increase in cellularity as the tumor becomes more malignant, leading to a rise in the volume fraction of restricted diffusion within the microenvironment and subsequently higher f_1 values in

LNM-positive rectal cancer patients [8, 20, 25]. Additionally, it has been reported that highly malignant LNM-positive tumors often display substantial necrosis and reduced extracellular space, which could hinder water proton diffusion and lead to lower f_3 values [19]. Furthermore, this study found no direct relationship between f_2 and LNM status in rectal cancer. This finding may be attributed to f_2 's lack of specificity in describing the cellularity of the tumor [20].

DKI quantitatively measures the complexity of tissue microstructure (K_{app}) and the diffusion of water

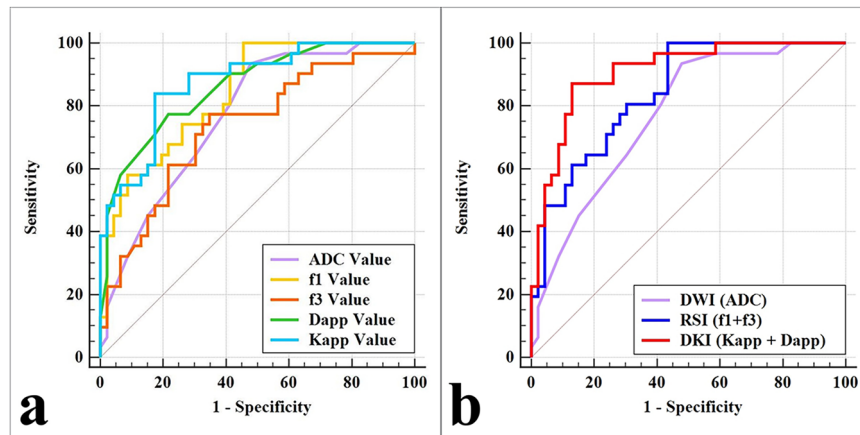


Fig. 3 The areas under receiver-operator characteristic (ROC) curves of different parameters (a) and different diffusion models (b)

Table 3 Predictive performance of different variables

Variables	AUC (95% CI)	p-value	Cutoff	Sensitivity	Specificity	Comparison with DKI
f_1	0.839 (0.738–0.913)	< 0.001	0.233	96.77%	54.35%	$Z = 2.360, p = 0.018$
f_2	0.519 (0.402–0.634)	0.784	/	/	/	/
f_3	0.733 (0.620–0.828)	< 0.001	0.305	77.42%	65.22%	$Z = 2.825, p = 0.005$
D_{app} ($\times 10^{-3} \text{mm}^2/\text{s}$)	0.860 (0.762–0.929)	< 0.001	1.200	77.42%	78.26%	$Z = 1.657, p = 0.098$
K_{app}	0.874 (0.779–0.939)	< 0.001	0.616	83.87%	82.61%	$Z = 1.499, p = 0.134$
DWI/ADC ($\times 10^{-3} \text{mm}^2/\text{s}$)	0.771 (0.661–0.859)	< 0.001	1.400	93.55%	52.17%	$Z = 3.453, p < 0.001$
RSI	0.842 (0.741–0.915)	< 0.001	/	96.77%	56.52%	$Z = 2.113, p = 0.035$
DKI	0.908 (0.820–0.962)	< 0.001	/	87.10%	86.96%	/

DWI = ADC, RSI = $f_1 + f_3$, DKI = $D_{app} + K_{app}$
 CI confidence interval

molecules within the tissues (D_{app}) [26, 27]. DKI has demonstrated clinical utility in differentiating LNM-positive from LNM-negative in other cancers, such as breast cancer [28] and cervical cancer [29]. Similar to evaluation in different cancers, the analysis of the current study revealed that LNM-negative rectal cancer patients exhibited a decrease in K_{app} and an increase in D_{app} compared to the LNM-positive group. Variations in tissue malignancy levels may significantly contribute to these results. Compared to LNM-negative tumors, LNM-positive tumors are more compact and exhibit characteristics such as hemorrhaging, necrosis, and higher tissue heterogeneity [28, 29]. These malignant characteristics impede the rate of water molecule diffusion and increase the deviation of the diffusion movement of water molecules, resulting in a decline in the D_{app} value and an increase in the K_{app} value.

This study compared the diagnostic performance of DKI, RSI, and DWI in assessing the LNM status of rectal cancer patients. The results showed that DKI had higher

diagnostic performance than RSI, followed by DWI. The DWI model exhibited the lowest diagnostic efficacy as it assumes a uniform Gaussian distribution of water molecules which does not effectively capture the complex and heterogenous nature of biological tissues due to variation in factors such as cellularity and tissue structure. The RSI model, in contrast to DWI, attempts to describe water diffusion as restricted, hindered and free diffusion, and thereby provides a more comprehensive picture of water molecule diffusion [19, 20]. As previously discussed, DKI is more sensitive to the diffusion motion of water molecules in tissues with a non-Gaussian distribution and measures cellularity and tissue structure changes. This enables an accurate and more realistic representation of the complex characteristics of rectal cancer lesions [26, 27].

Selecting the b-value is one of the most important factors that influences the diagnostic performance of the RSI model. Some reports have indicated that RSI fitted using 4–7 b-values with a maximum of $4000 \text{mm}^2/\text{s}$ maintained

superior performance [30, 31]. However, Felker et al demonstrated that a combination of fewer and smaller b-values (four b-values up to a maximum of 1400 mm²/s) could also be employed and a reliable RSI fit could be achieved [32]. This study selected twelve b-values up to 2000 mm²/s to optimize scanning time and image quality to fit the RSI. Similar to a study by Xiong et al [20], this study showed fair diagnostic performance of RSI, providing evidence that the selected b-value was a reliable tool in assessing rectal cancer. However, there is currently no consensus on the optimal b-value for RSI model fitting, and further studies with larger sample sizes are needed to establish standardized protocols.

The present study has some limitations. First, it was conducted at a single institution with a limited number of participants. Second, the RSI, DKI, and DWI were all based on echo planar imaging, resulting in a lack of visualization of small lesions. Finally, the choice of b-value for RSI images may require further optimization to ensure optimal image quality and diagnostic accuracy.

Conclusion

The three-compartment RSI model was able to differentiate between LNM-positive and LNM-negative rectal cancers. Compared to conventional DWI, the RSI model exhibited superior diagnostic performance, but weaker than that of DKI. These findings suggest that the RSI model has the potential to serve as a promising biomarker for guiding effective treatment strategies.

Abbreviations

ADC	Apparent diffusion coefficient
AUC	Area under the receiver operating characteristic curve
DKI	Diffusion kurtosis imaging
DWI	Diffusion-weighted imaging
LNM	Lymph node metastases
LR	Logistic regression
MRI	Magnetic resonance imaging
RSI	Restriction spectrum imaging

Acknowledgements

We acknowledge the support received from the Key Research Projects of Higher Education Institutions in Henan Province.

Author contributions

R.Y. and D.H.: Investigation, Funding acquisition, Supervision. H.Y. and W.L.: Data curation, Roles/Writing-original draft Formal analysis. Q.X., C.S., and J.R.: Formal analysis. D.W. and Z.L.: Methodology. K.W.: Validation, Writing-review & editing.

Funding

The Key Research Projects of Higher Education Institutions in Henan Province (No. 24B320017), the Key Project of Henan Province Medical Science and Technology Project (Nos. LHGJ20210498, LHGJ20230505).

Data availability

All data are with the corresponding author and can be obtained by mail if necessary.

Declarations

Ethics approval and consent to participate

This prospective study had approval from our hospital's ethics review committee and each patient provided signed informed consent.

Consent for publication

All participants provided written informed consent.

Competing interests

K.W., who is an employee of GE Healthcare, gave guidance to this paper in terms of technical parameters and language embellishment. The remaining authors declare no relationships with any companies whose products or services may be related to the subject matter of the article. No conflicts of interest between the two corresponding authors or between the two research projects.

Author details

¹Department of MR, The First Affiliated Hospital, Xinxiang Medical University, Weihui, China. ²Hematology Laboratory, The First Affiliated Hospital of Xinxiang Medical University, Xinxiang, China. ³Department of Radiology, People's Hospital of Zhengzhou, Zhengzhou 450000, PR China. ⁴MR Research China, GE Healthcare, Beijing, China.

Received: 16 June 2024 Accepted: 22 October 2024

Published online: 19 December 2024

References

- Siegel RL, Miller KD, Wagle NS, Jemal A (2023) Cancer statistics, 2023. *CA Cancer J Clin* 73:17–48. <https://doi.org/10.3322/caac.21763>
- Benson AB, Venook AP, Al-Hawary MM et al (2022) Rectal cancer, version 2.2022, NCCN clinical practice guidelines in oncology. *J Natl Compr Canc Netw* 20:1139–1167. <https://doi.org/10.6004/jnccn.2022.0051>
- Kroon HM, Hoogervorst LA, Hanna-Rivero N et al (2022) Systematic review and meta-analysis of long-term oncological outcomes of lateral lymph node dissection for metastatic nodes after neoadjuvant chemoradiotherapy in rectal cancer. *Eur J Surg Oncol* 48:1475–1482. <https://doi.org/10.1016/j.ejso.2022.04.016>
- Schaap DP, Boogerd LSF, Konishi T et al (2021) Rectal cancer lateral lymph nodes: multicentre study of the impact of obturator and internal iliac nodes on oncological outcomes. *Br J Surg* 108:205–213. <https://doi.org/10.1093/bjs/znaa009>
- Smith FM, Winter D (2017) Pathologic complete response of primary tumor following preoperative chemoradiotherapy for locally advanced rectal cancer: long-term outcomes and prognostic significance of pathologic nodal status (KROG 09-01). *Ann Surg* 265:e27–e28. <https://doi.org/10.1097/SLA.0000000000000462>
- Tapan U, Ozbayrak M, Tatli S (2014) MRI in local staging of rectal cancer: an update. *Diagn Interv Radiol* 20:390–398. <https://doi.org/10.5152/dir.2014.13265>
- Arian A, Taher HJ, Suhail Najm Alareer H, Aghili M (2023) Value of conventional MRI, DCE-MRI, and DWI-MRI in the discrimination of metastatic from non-metastatic lymph nodes in rectal cancer: a systematic review and meta-analysis study. *Asian Pac J Cancer Prev* 24:401–410. <https://doi.org/10.31557/APJCP.2023.24.2.401>
- Cho EY, Kim SH, Yoon JH et al (2013) Apparent diffusion coefficient for discriminating metastatic from non-metastatic lymph nodes in primary rectal cancer. *Eur J Radiol* 82:e662–e668. <https://doi.org/10.1016/j.ejrad.2013.08.007>
- Xu Q, Xu Y, Wang J, Sun H, Lin J, Xie S (2023) Distinguishing mesorectal tumor deposits from metastatic lymph nodes by using diffusion-weighted and dynamic contrast-enhanced magnetic resonance imaging in rectal cancer. *Eur Radiol* 33:4127–4137. <https://doi.org/10.1007/s00330-022-09328-8>
- Heijnen LA, Lambregts DM, Mondal D et al (2013) Diffusion-weighted MR imaging in primary rectal cancer staging demonstrates but does not characterise lymph nodes. *Eur Radiol* 23:3354–3360. <https://doi.org/10.1007/s00330-013-2952-5>

11. Surov A, Meyer HJ, Pech M, Powerski M, Omari J, Wienke A (2021) Apparent diffusion coefficient cannot discriminate metastatic and non-metastatic lymph nodes in rectal cancer: a meta-analysis. *Int J Colorectal Dis* 36:2189–2197. <https://doi.org/10.1007/s00384-021-03986-8>
12. Jensen JH, Helpert JA, Ramani A, Lu H, Kaczynski K (2005) Diffusional kurtosis imaging: the quantification of non-Gaussian water diffusion by means of magnetic resonance imaging. *Magn Reson Med* 53:1432–1440. <https://doi.org/10.1002/mrm.20508>
13. Meng N, Wang X, Sun J et al (2020) Application of the amide proton transfer-weighted imaging and diffusion kurtosis imaging in the study of cervical cancer. *Eur Radiol* 30:5758–5767. <https://doi.org/10.1007/s00330-020-06884-9>
14. Jensen JH, Helpert JA (2010) MRI quantification of non-Gaussian water diffusion by kurtosis analysis. *NMR Biomed* 23:698–710. <https://doi.org/10.1002/nbm.1518>
15. Wang C, Yu J, Lu M, Li Y, Shi H, Xu Q (2022) Diagnostic efficiency of diffusion sequences and a clinical nomogram for detecting lymph node metastases from rectal cancer. *Acad Radiol* 29:1287–1295. <https://doi.org/10.1016/j.acra.2021.10.009>
16. Yu J, Dai X, Zou HH et al (2018) Diffusion kurtosis imaging in identifying the malignancy of lymph nodes during the primary staging of rectal cancer. *Colorectal Dis* 20:116–125. <https://doi.org/10.1111/codi.13835>
17. White NS, McDonald C, Farid N et al (2014) Diffusion-weighted imaging in cancer: physical foundations and applications of restriction spectrum imaging. *Cancer Res* 74:4638–4652. <https://doi.org/10.1158/0008-5472.CAN-13-3534>
18. Eng SE, Basasie B, Lam A et al (2024) Prospective comparison of restriction spectrum imaging and non-invasive biomarkers to predict upgrading on active surveillance prostate biopsy. *Prostate Cancer Prostatic Dis* 27:65–72. <https://doi.org/10.1038/s41391-022-00591-w>
19. Qin Y, Tang C, Hu Q et al (2023) Quantitative assessment of restriction spectrum MR imaging for the diagnosis of breast cancer and association with prognostic factors. *J Magn Reson Imaging* 57:1832–1841. <https://doi.org/10.1002/jmri.28468>
20. Xiong Z, Geng Z, Lian S et al (2022) Discriminating rectal cancer grades using restriction spectrum imaging. *Abdom Radiol (NY)* 47:2014–2022. <https://doi.org/10.1007/s00261-022-03500-w>
21. Amin MB, Greene FL, Edge SB et al (2017) The eighth edition AJCC cancer staging manual: continuing to build a bridge from a population-based to a more “personalized” approach to cancer staging. *CA Cancer J Clin* 67:93–99. <https://doi.org/10.3322/caac.21388>
22. Shieh G (2016) Choosing the best index for the average score intraclass correlation coefficient. *Behav Res Methods* 48:994–1003. <https://doi.org/10.3758/s13428-015-0623-y>
23. Meng N, Song C, Sun J et al (2024) Amide proton transfer-weighted imaging and stretch-exponential model DWI based 18F-FDG PET/MRI for differentiation of benign and malignant solitary pulmonary lesions. *Cancer Imaging* 24:33. <https://doi.org/10.1186/s40644-024-00677-9>
24. Brunsing RL, Schenker-Ahmed NM, White NS et al (2017) Restriction spectrum imaging: an evolving imaging biomarker in prostate MRI. *J Magn Reson Imaging* 45:323–336. <https://doi.org/10.1002/jmri.25419>
25. Andreassen MMS, Rodríguez-Soto AE, Conlin CC et al (2021) Discrimination of breast cancer from healthy breast tissue using a three-component diffusion-weighted MRI model. *Clin Cancer Res* 27:1094–1104. <https://doi.org/10.1158/1078-0432.CCR-20-2017>
26. Jiang JX, Tang ZH, Zhong YF, Qiang JW (2017) Diffusion kurtosis imaging for differentiating between the benign and malignant sinonasal lesions. *J Magn Reson Imaging* 45:1446–1454. <https://doi.org/10.1002/jmri.25500>
27. Zhu L, Pan Z, Ma Q et al (2017) Diffusion kurtosis imaging study of rectal adenocarcinoma associated with histopathologic prognostic factors: preliminary findings. *Radiology* 284:66–76. <https://doi.org/10.1148/radiol.2016160094>
28. Zhou Z, Chen Y, Zhao F et al (2023) Predictive value of intravoxel incoherent motion combined with diffusion kurtosis imaging for breast cancer axillary lymph node metastasis: a retrospective study. *Acta Radiol* 64:951–961. <https://doi.org/10.1177/02841851221107626>
29. Huang Q, Wang Y, Meng X et al (2023) Amide proton transfer-weighted imaging combined with ZOOMit diffusion kurtosis imaging in predicting lymph node metastasis of cervical cancer. *Bioengineering* 10:331. <https://doi.org/10.3390/bioengineering10030331>
30. Krishnan AP, Karunamuni R, Leyden KM et al (2017) Restriction spectrum imaging improves risk stratification in patients with glioblastoma. *AJNR Am J Neuroradiol* 38:882–889. <https://doi.org/10.3174/ajnr.A5099>
31. White NS, McDonald CR, Farid N, Kuperman JM, Kesari S, Dale AM (2013) Improved conspicuity and delineation of high-grade primary and metastatic brain tumors using “restriction spectrum imaging”: quantitative comparison with high B-value DWI and ADC. *AJNR Am J Neuroradiol* 34:958–964. <https://doi.org/10.3174/ajnr.A3327>
32. Felker ER, Raman SS, Shakeri S et al (2019) Utility of restriction spectrum imaging among men undergoing first-time biopsy for suspected prostate cancer. *AJR Am J Roentgenol* 213:365–370. <https://doi.org/10.2214/AJR.18.20836>

Publisher's Note

Springer Nature remains neutral with regard to jurisdictional claims in published maps and institutional affiliations.